

Supporting Information to:

**Self-assembly and liquid-crystalline supramolecular organizations
of semifluorinated block co-dendritic supermolecules**

Izabela Bury,^a Benoît Heinrich,^a Cyril Bourgogne,^a Georg H. Mehl,^b Daniel Guillon^a and
Bertrand Donnio,^{*a}

^aInstitut de Physique et Chimie des Matériaux de Strasbourg – IPCMS, UMR 7504 –
CNRS/Université de Strasbourg, 23, rue du Loess, BP 43, F-67034 Strasbourg Cedex 2,
France.

^bUniversity of Hull, Department of Chemistry, Cottingham Road, Hull, HU67RX, UK

Corresponding author : e-mail: bdonnio@ipcms.u-strasbg.fr, tel: +33 388107156, fax: +33
388107246

TABLE OF CONTENT

- 1. EXPERIMENTAL TECHNIQUES**
- 2. SELECTION OF OPTICAL TEXTURES**
- 3. MOLECULAR DYNAMICS**
- 4. X-RAY DIFFRACTION**
- 5. DIFFERENTIAL SCANNING CALORIMETRY**

1. EXPERIMENTAL TECHNIQUES

^1H , ^{19}F and ^{13}C NMR spectra were recorded on a Bruker AVANCE 300 (300MHz) spectrometer (IPCMS) and on a Bruker DRX 500 (500MHz) at University of Hull. The internal references of the spectrum correspond to the peak of the non deuterated solvent (CDCl_3 7.27ppm, THF- d_8 1.7 and 3.55ppm, or $(\text{CD}_3)_2\text{CO}$ 2.04 and 2.77ppm).

MALDI-TOF spectra were recorded on a Bruker biflex III spectrometer in a dithranol matrix (1,8,9-anthracenetriol).

Elemental analyses were realized at the Charles Sadron Institute Strasbourg (France) and at the chemistry department of the University of Hull (England).

The optical textures of the mesophases were studied with a Leitz polarizing microscope equipped with a Mettler FP82 hot-stage and an FP80 central processor.

The transition temperatures and enthalpies were measured by differential scanning calorimetry with a TA Instruments DSC-Q1000 instrument operated at a scanning rates of 1 to 5°C min^{-1} on heating and on cooling.

The TGA measurements were carried out on a SDTQ 600 apparatus at scanning rate of $10^\circ\text{C min}^{-1}$.

The XRD patterns were obtained with three different experimental set-ups (I, II, III). In all cases, a linear monochromatic $\text{Cu-K}\alpha_1$ beam ($\lambda = 1.5405\text{\AA}$) was obtained using a sealed-tube generator (900W) equipped with a bent quartz monochromator. . In all cases, the crude powder was filled in Lindemann capillaries of 1 mm diameter and 10 μm wall-thickness. An initial set of diffraction patterns was recorded on an image plate (scanned by STORM 820 from Molecular Dynamics with 50 μm resolution); periodicities up to 80 \AA can be measured, and the sample temperature controlled to within $\pm 0.3^\circ\text{C}$ from 20 to 350°C . The second set of diffraction patterns was recorded with a curved Inel CPS 120 counter gas-filled detector linked to a data acquisition computer; periodicities up to 70 \AA can be measured, and the sample temperature controlled to within $\pm 0.01^\circ\text{C}$ from 20 to 200°C . Alternatively, patterns were also recorded on an image plate; periodicities up to 120 \AA can be measured. Finally, the last set of diffraction patterns was recorded on image plate, and periodicities up to 350 \AA can be measured, and the sample temperature controlled to within $\pm 0.1^\circ\text{C}$ from 20 to 200°C . In each case, exposure times were varied from 1 to 24 h.

The molecular modeling calculations were performed on an SGI Origin 200 4 CPU computer and on an SGI Octane² workstation using the DISCOVER 3 molecular mechanics package

from Accelrys (www.accelrys.com) with the pcff force field. For both smectic and columnar models, prior to the dynamics, the systems were minimized to a gradient of 0.5kcal mol^{-1} . The simulation then consisted of a 100ps isotherm at 373K in the NVT-PBC ensemble and with a 1 fs time step.

2. SELECTION OF OPTICAL TEXTURES

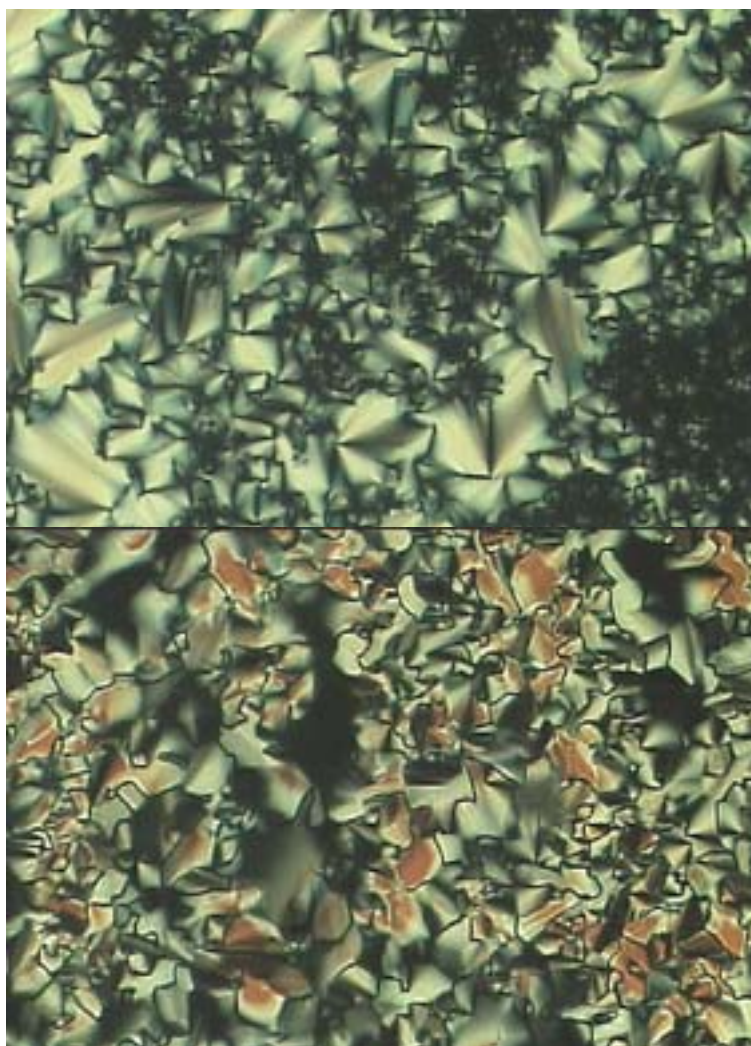


Figure S1 Optical textures of the Col_r phase of $(3,4)^1(3,5)^2\text{H-F}^1$ at $T=42^\circ\text{C}$ and 48°C (on heating)



Figure S2 Optical texture (cylindrical domains) of the Col_h phase of (3,4)¹(3,5)²H-F¹ at T=43°C (on cooling)

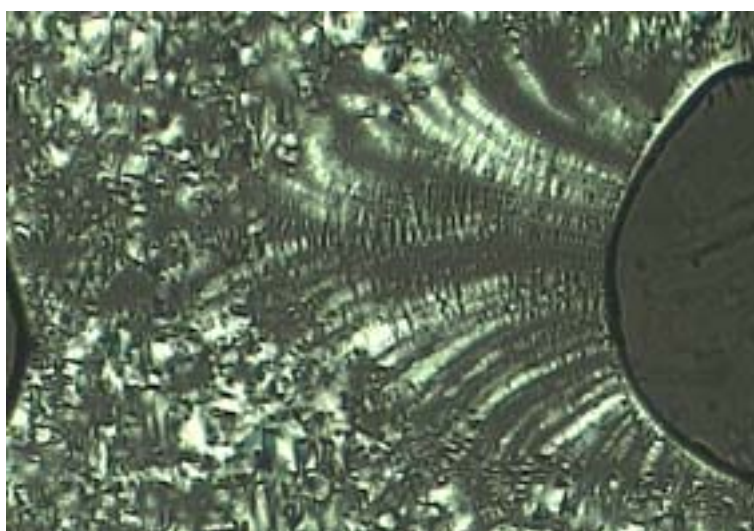


Figure S3 Optical texture (myelinic) of the lamellar phase (Lam) of (3,4,5)¹H-F² at T=47°C (on cooling)

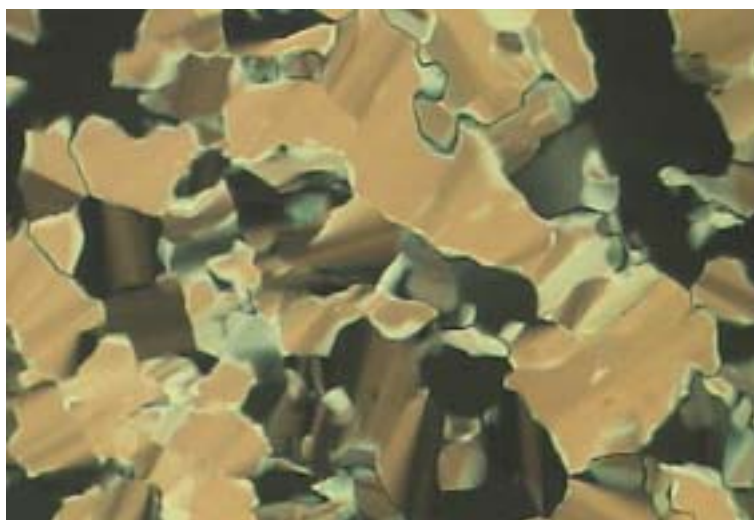


Figure S4 Optical texture of the Col_{h1} phase of (3,4,5)¹(3,5)¹H-F² at T=60°C (on cooling)

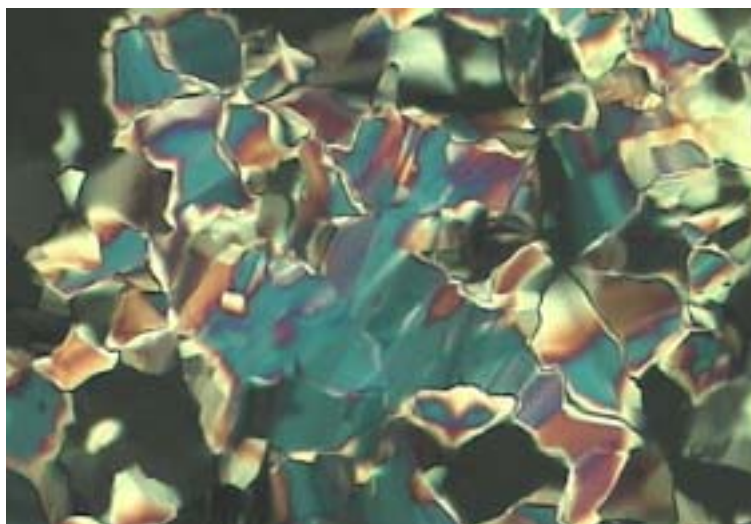


Figure S5 Optical texture of the Col_{hl} phase near the transition of $(3,4,5)^1(3,5)^1H-F^2$ at $T=30^\circ C$ (on cooling)

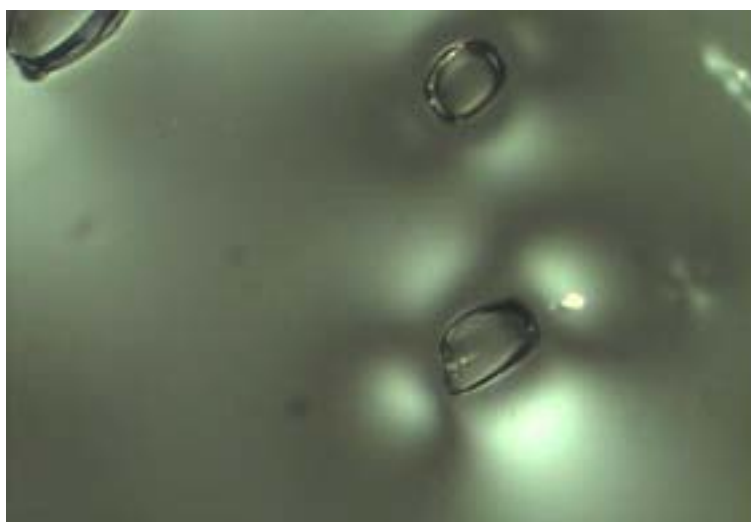


Figure S6 Low birefringence, optical texture of the monoclinic phase of $(3,4,5)^1(3,5)^2H-F^2$ at $T=40^\circ C$ (on cooling)

3. MOLECULAR DYNAMICS

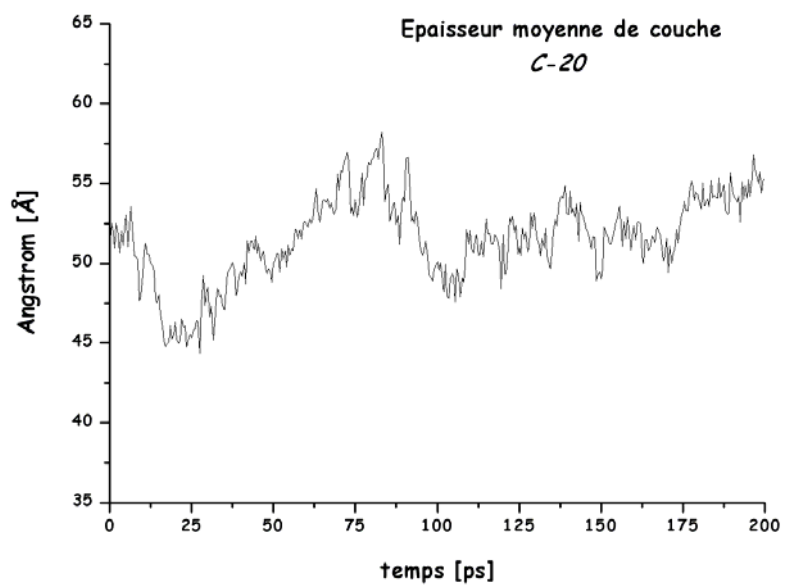


Figure S7 Variation of the bilayer thickness of the lamellar phase of (3,4,5)- $H-F^2$ (C20) as a function of time.

4. X-RAY DIFFRACTION

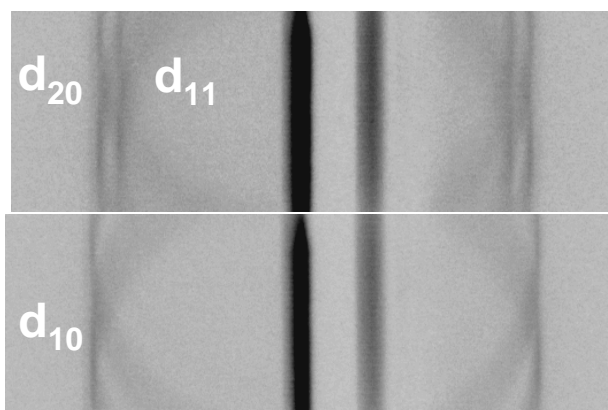
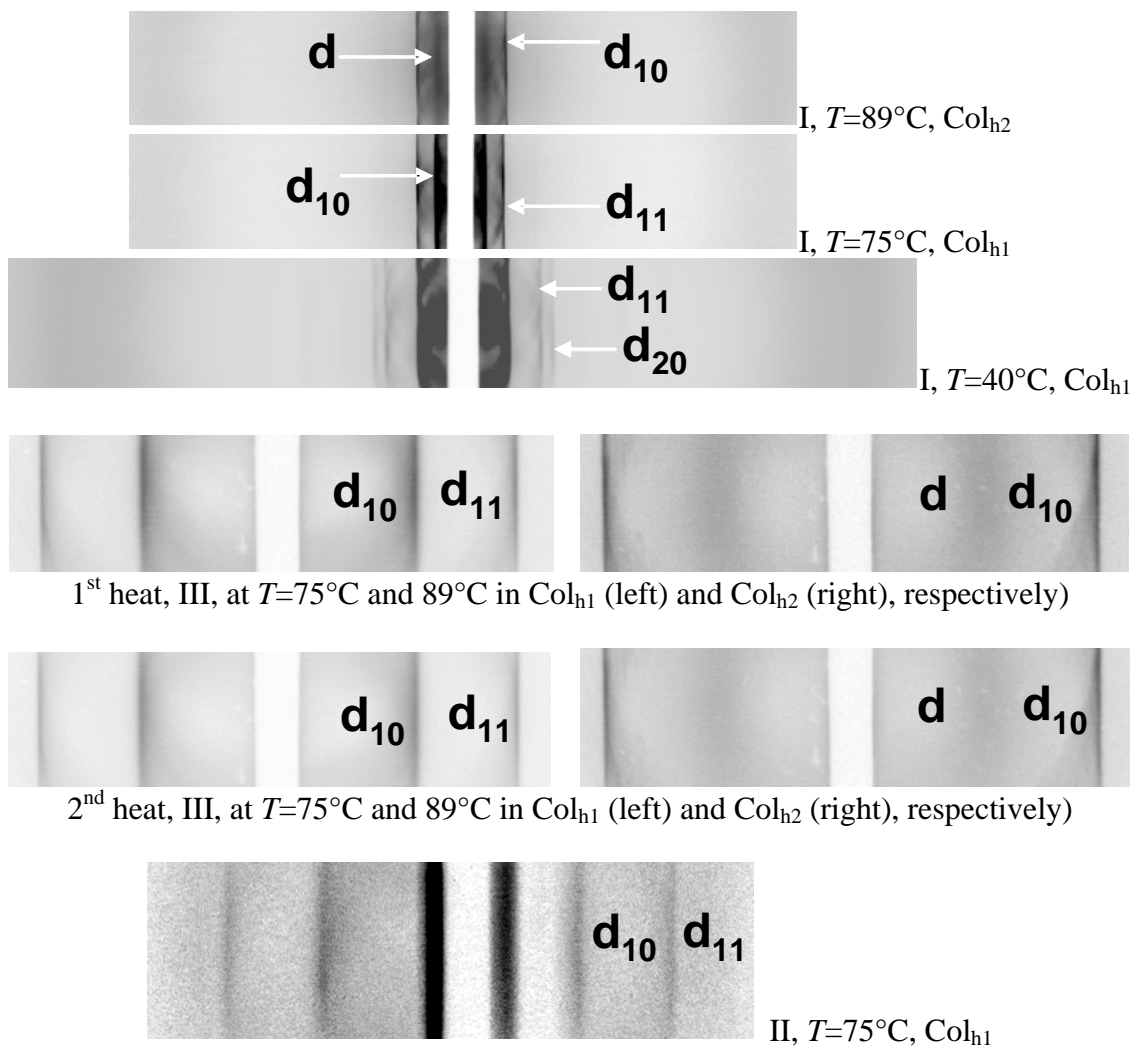


Figure S8 Small-angle X-ray diffraction patterns (image plates, setup II) of the columnar rectangular phase, Col_r , at $T=30^\circ\text{C}$ (top), and of columnar hexagonal phase, Col_h , at $T=45^\circ\text{C}$ (bottom) of $(3,4)^1(3,5)^2\text{H-F}^1$.



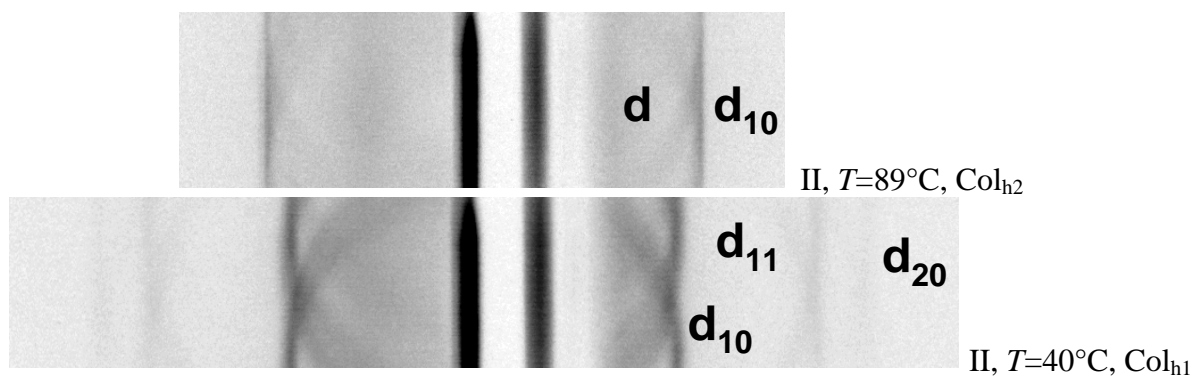


Figure S9 Small-angle X-ray diffraction patterns (image plates, setups I, II and III) of the columnar hexagonal phases, Col_{h1} and Col_{h2}, of $(3,4)^1(3,5)^2\mathbf{H-F}^2$.

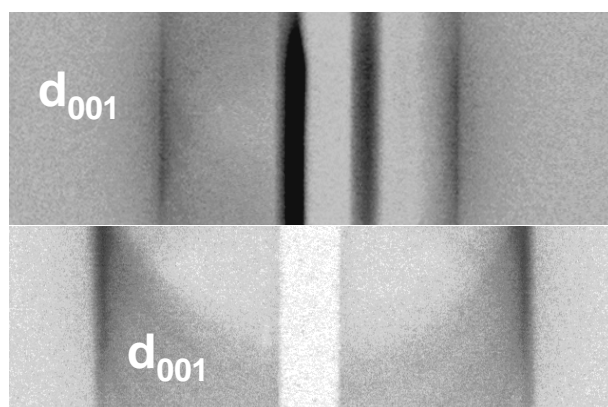


Figure S10 Small-angle X-ray diffraction patterns (image plates, setups II and III) of the lamellar phase of $(3,4,5)^1\mathbf{H-F}^2$ ($T=45^\circ\text{C}$).

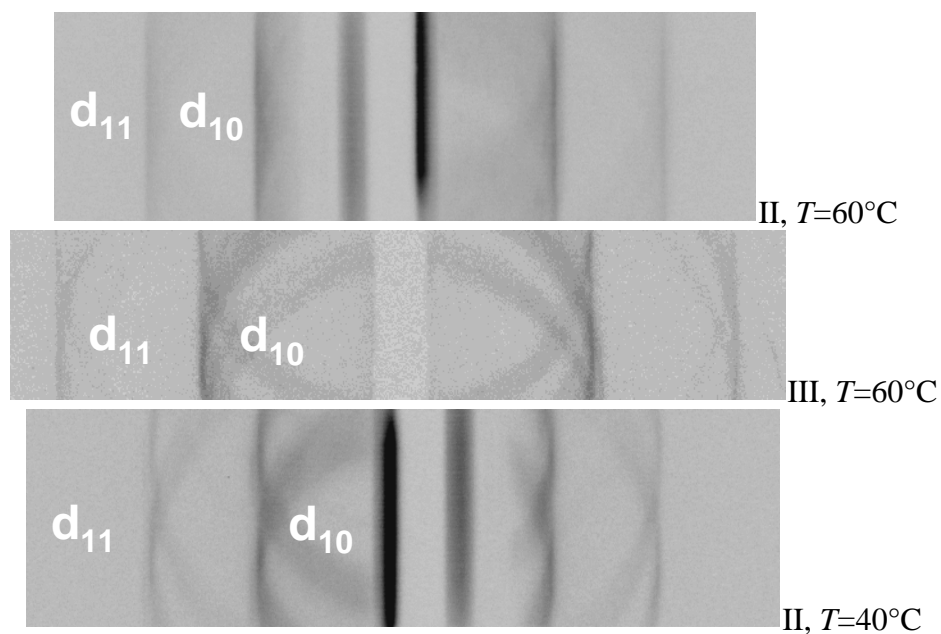


Figure S11 Small-angle X-ray diffraction patterns (image plates, setups II and III) of the columnar hexagonal phase of $(3,4,5)^1(3,5)^1\mathbf{H-F}^2$.

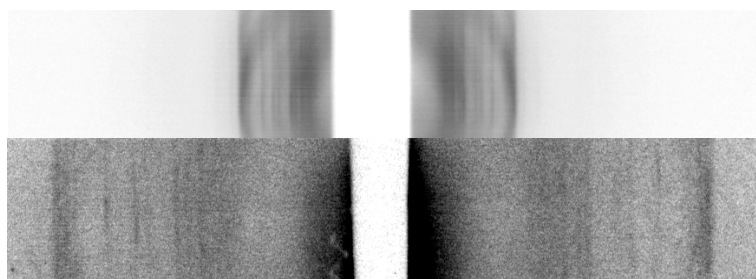


Figure S12 Small-angle X-ray diffraction patterns (image plates, setups I and II) of the monoclinic phase of $(3,4,5)^1(3,5)^2\text{H-F}^2$ ($T=45^\circ\text{C}$).

Indexation of the monoclinic phase of $(3,4,5)^1(3,5)^2\text{H-F}^2$ at $T = 45^\circ\text{C}$

Table S1. Monoclinic lattice n°1

N°	$2\theta_{\text{obs}}$ °	d_{obs} Å	I	hkl	$2\theta_{\text{cal}}$ °	d_{cal} Å
1	1.25	70.5	W	0 0 2	1.249	70.65
2	1.36	64.7	M	1 -1 0	1.347	65.55
3	1.52	58.0	S	1 0 0	1.514	58.30
4	1.65	53.6	W	1 0 -1 / 1 0 1	1.638	53.89
5	1.75	50.5	S	0 1 0	1.758	50.22
6	2.00	44.2	W	1 0 -2 / 1 0 2	1.963	44.97
7	2.11	41.8	W	0 1 -2 / 0 1 2	2.156	40.93
				2 -1 0	2.263	39.00
8	2.33	37.8	M	2 -1 -1 / 2 -1 1	2.347	37.60
9	2.70	32.7	W	2 -2 0	2.693	32.77
				1 -2 0	2.741	32.20
10	2.76	31.9	S	2 -2 -1 / 2 -2 1	2.765	31.93
11	2.97	29.8	VW	2 -2 -2 / 2 -2 2	2.969	29.73
12	3.26	27.1	VW	1 1 -2 / 1 1 2	3.242	27.23
				2 0 -2 / 2 0 2	3.276	26.95

$a = 78.5(74)$ Å; $b = 67.6(84)$ Å; $c = 141.3$ Å; $\alpha = \beta = 90^\circ$; $\gamma = 132.1^\circ$; $V = 557(568)$ Å³; $A = a \times b \sin(\gamma) = 3946$ Å²

Table S2. Monoclinic lattice n°2

N°	$2\theta_{\text{obs}}$ °	d_{obs} Å	I	hkl	$2\theta_{\text{cal}}$ °	d_{cal} Å
1	1.25	70.5	W	0 0 2	1.249	70.65
2	1.36	64.7	M	1 -1 0	1.347	65.54
3	1.52	58.0	S	1 0 0	1.511	58.40
				1 0 -1 / 1 0 1	1.635	53.97
4	1.65	53.6	W	0 1 0	1.645	53.66
5	1.75	50.5	S	0 1 -1 / 0 1 1	1.760	50.16
6	2.00	44.2	W	1 0 -2 / 1 0 2	1.961	45.01
7	2.11	41.8	W	0 1 -2 / 0 1 2	2.066	42.73
8	2.33	37.8	M	2 -1 0	2.343	37.67
9	2.70	32.7	W	2 -2 0	2.694	32.77
10	2.76	31.9	S	2 -2 -1 / 2 -2 1	2.765	31.92
				1 1 -1 / 1 1 -1	2.925	30.17
11	2.97	29.8	VW	2 -2 -2 / 2 -2 2	2.970	29.73
12	3.26	27.1	VW	2 0 -2 / 2 0 2	3.271	26.99
				0 2 0	3.290	26.83

$a = 75.9(033)$ Å; $b = 69.7(427)$ Å; $c = 141.3$ Å; $\alpha = \beta = 90^\circ$; $\gamma = 129.7^\circ$; $V = 575(511)$ Å³; $A = a \times b \sin(\gamma) = 4073$ Å²

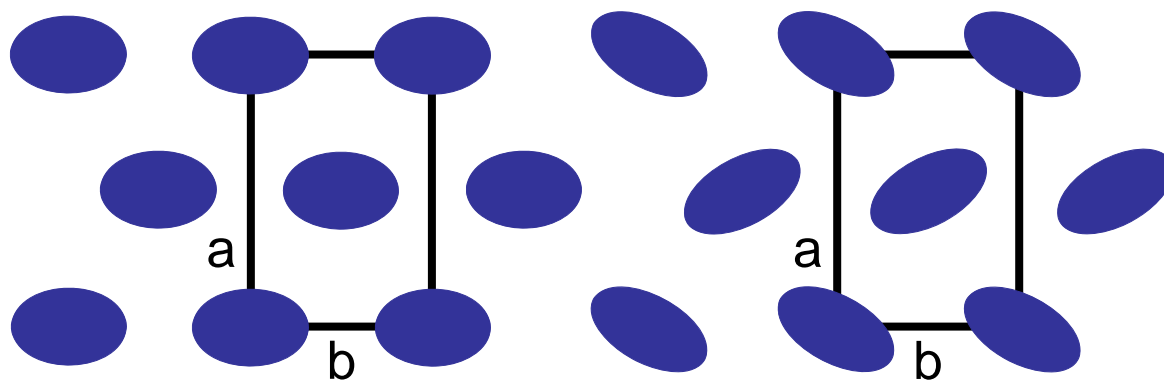


Figure S13 Schematic representation of the two rectangular symmetries, centred, $c2mm$, and the non-centred, $p2gg$.

5. DIFFERENTIAL SCANNING CALORIMETRY

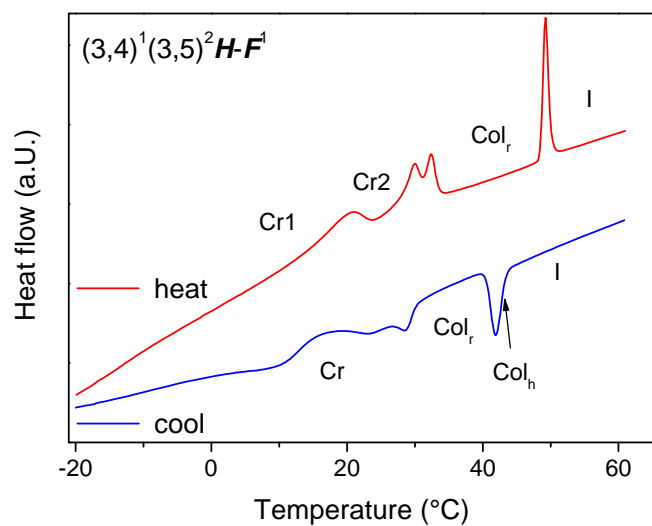


Figure S14 DSC traces of $(3,4,5)^1(3,5)^1H-F^2$ (2nd cooling cycle, 3rd heating cycle).

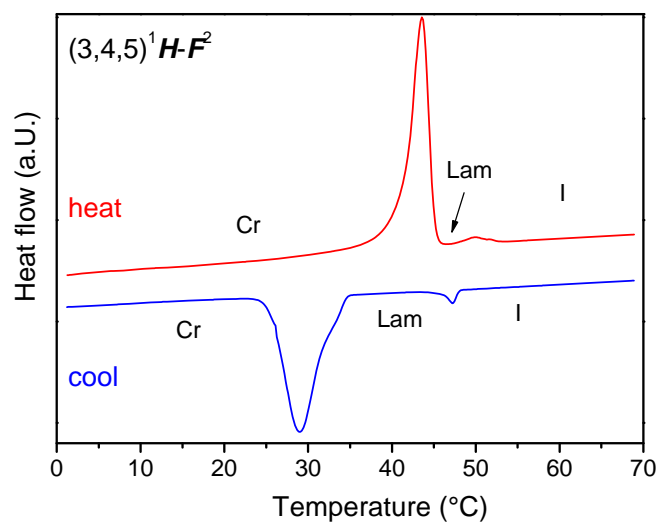


Figure S15 DSC traces of $(3,4,5)^1H-F^2$ (2nd cooling cycle, 3rd heating cycle).

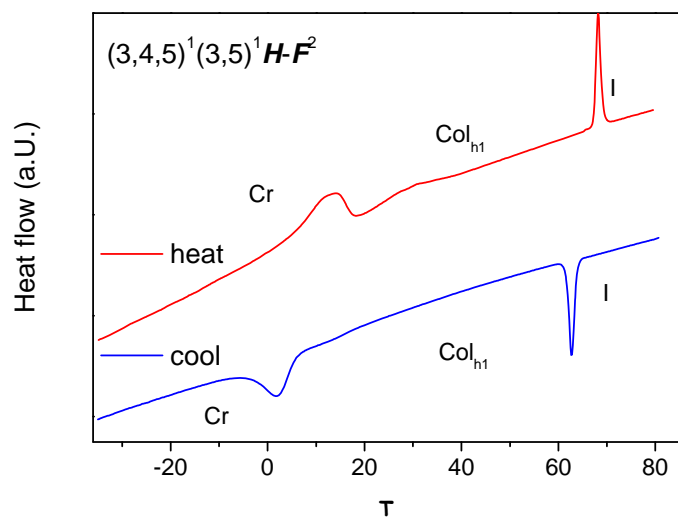


Figure S16 DSC traces of $(3,4,5)^1(3,5)^1\text{H-F}^2$ (2nd cooling cycle, 3rd heating cycle).

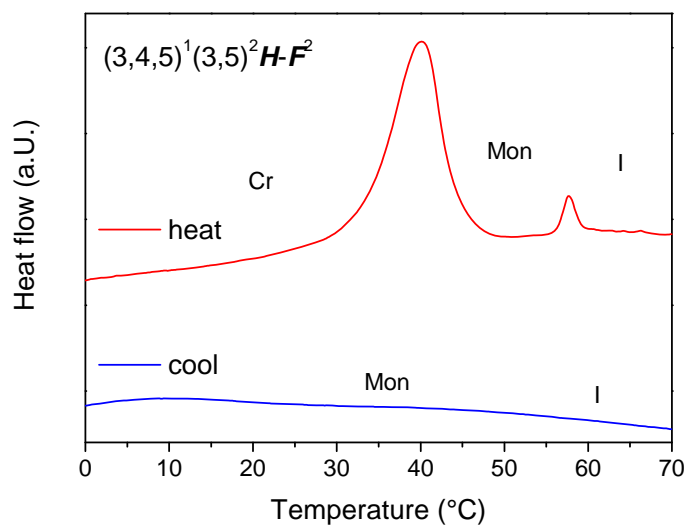


Figure S17 DSC traces of $(3,4,5)^1(3,5)^2\text{H-F}^2$ (2nd cooling cycle, 3rd heating cycle).